World Academy of Science, Engineering and Technology
International Journal of Aerospace and Mechanical Engineering
Vol:6, No:3, 2012

Numerical Analysis of the Performance of a Shrouded Vertical-Axis Water Turbine based on the NACA 0025 Blade Profile

M. Raciti Castelli, S. De Betta, E. Benini

***Abstract*—**This paper presents a numerical analysis of the performance of a five-bladed Darrieus vertical-axis water turbine, based on the NACA 0025 blade profile, for both bare and shrouded configurations. A complete campaign of 2-D simulations, performed for several values of tip speed ratio and based on RANS unsteady calculations, has been performed to obtain the rotor torque and power curves. Also the effect of a NACA-shaped central hydrofoil has been investigated, with the aim of evaluating the impact of a solid blockage on the performance of the shrouded rotor configuration.

The beneficial effect of the shroud on rotor overall performances has clearly been evidenced, while the adoption of the central hydrofoil has proved to be detrimental, being the resulting flow slow down (due to the presence of the obstacle) much higher with respect to the flow acceleration (due to the solid blockage effect).

***Keywords*—**CFD, vertical axis water turbine, shroud, NACA 0025

I. Introduction and Background

CONVENTIONAL hydroelectricity, one of the dominant forms of renewable Energy, is facing a scarcity of suitable installation sites just as the need for renewables is becoming greater. As a consequence, alternative forms of hydropower must be pursued, in order to tap the hydroelectric energy potential of the world. Kinetic hydropower, using submerged turbines in existing currents to produce electricity, is one of such alternatives. The main advantage of a kinetic hydropower turbine consists in its possible operation without the need of large infrastructures, such as dams and powerhouses, thus reducing both cost and deployment time. Moreover, with no reservoir or spillways, the environmental impact is minimal [1].

The process of hydrokinetic energy conversion implies the adoption of kinetic energy contained in river streams, tidal currents, or other man-made waterways for the generation of electricity. This emerging class of renewable energy technology is being strongly recognized as a unique and unconventional solution that falls within the realms of both in-land water resource and marine energy [2].An important advantage of ocean and tidal currents is that a highly predictable power output can be achieved.

Marco Raciti Castelli is a Research Associate at the Department of Mechanical Engineering of the University of Padua, Via Venezia 1, 35131 Padova, Italy (e-mail: marco.raciticastelli@unipd.it).

Stefano De Betta has completed his M.Sc. in Aerospace Engineering at the University of Padua, Via Venezia 1, 35131 Padova, Italy.

Ernesto Benini is an Associate Professor at the Department of Mechanical Engineering of the University of Padua, Via Venezia 1, 35131 Padova, Italy (e-mail: ernesto.benini@unipd.it).

Apart from that, energy extraction from unregulated watercourses presents several aspects in common with wind power, the main difference being the density of water, which is approximately 800 times the density of air. This means that a turbine rotor for underwater applications can be much smaller than a wind turbine of the same rated power [3].

A way to increase the power extraction from a wind or water turbine consists of the adoption of an augmentation channel. If a turbine is placed in such a channel, the velocity around the rotor would be increased, leading to an enhancement of the generated power [4]. Khan et al. [2] gave an overview of some possible geometrical solutions for a duct channel, making distinction between ducts for horizontal and vertical axis turbines.

Gaden and Bibeau [1] investigated the use of a shroud to enhance the power production of a turbine. A series of numerical experiments, using a momentum source turbine model was performed, determining that the power output can be increased by a factor 3.1 with a diffuser mounted at the trailing edge. Furthermore, it was found that the diffuser presents an optimum size, beyond which the power production does not increase significantly.

Kirke [5] placed a Darrieus turbine in a duct to study the augmentation in power extraction. A performance increment by a factor of about 3 was determined when the duct was added. Moreover, the maximum energy conversion by ducted turbines resulted not to be subjected to the Betz limit, since a suitable shaped duct can increase the available pressure drop across the turbine. Besides, a duct presents several practical advantages, including improved safety, protection from weed growth, increased speed and reduced turbine and gearbox size for a given power output.

Roa et al. [6] discussed the benefit of introducing a channeling device near a Darrieus-type cross flow water turbine. A series of numerical and experimental analysis was performed, determining an increment in efficiency of a factor from 2.7 to 4.9 numerically and from 2.5 to 3.75 experimentally. The differences between numerical and experimental data were attributed to 3D effects, such as blade tip vortices and drag effects at the blade-spoke junction. It was also proved that, if a turbine is equipped with a channeling device, the blades harness more torque, an acceleration of the flow due to a larger absorbed stream tube is observed and the torque distribution is smoothed over a full rotor revolution.Maitre et al. [7] operated a series of numerical

analysis to optimize a symmetrical two-foiled channeling device for Darrieus type cross flow water turbines.

The aim of the present work is to determine the effect of the presence of a shroud near a five-bladed Darrieus vertical-axis water turbine. Several numerical analyses were performed for different values of tip speed ratio. Three cases were analyzed:

1. a bare rotor configuration;
2. a shrouded rotor configuration;
3. a shrouded rotor configuration, presenting a NACA 0060 shaped central device, in order to increase the blockage of the water current, thus further increasing its velocity.

II. Model Geometry

The aim of the present work is to numerically analyze the fluid-dynamic of a five-bladed rotor in bare and shrouded configuration. The main geometrical features of the rotor are summarized in Table I.

TABLE I
MAIN GEOMETRICAL FEATURES OF THE ANALYZED ROTOR

Denomination	Value
D_{rotor} [mm]	1030
H_{rotor} [mm]	1 (2D simulation)
Blade profile	NACA 0025
c [mm]	85.8

Rotor azimuthal position was identified by the angular coordinate of the pressure center of blade No. 1 (assumed to be at 0.25·c for a NACA 0025 profile), starting between the 2nd and 3rd Cartesian plane octants, as can be seen from Fig. 1.

Fig. 2 represents the geometry of the analyzed rotor, including the shroud, for the configuration without the NACA shaped central axis.

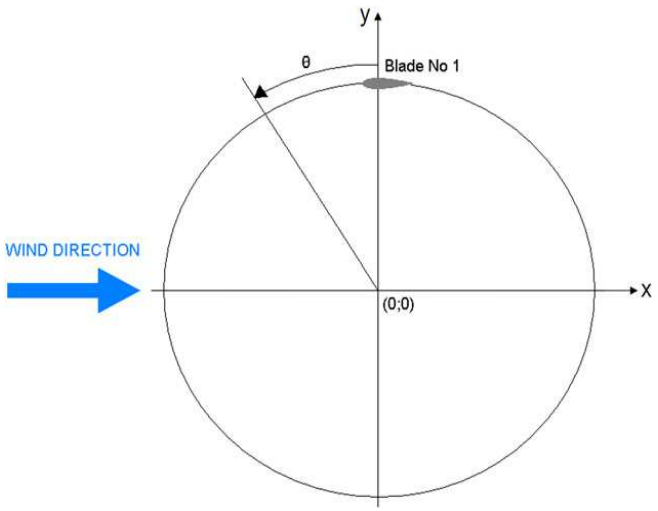

Fig. 1 Azimuthal coordinate of blade No.1 center of pressure

III. Description of the Numerical Flow Field

As the aim of the present work was to reproduce the operation of a rotating machine, the use of moving sub-grids was necessary. In particular, the discretization of the computational domain into macro-areas led to two distinct sub-grids:

- a rectangular outer zone, determining the overall calculation domain, with a circular opening centered on the turbine rotational axis, which was identified as *Water Tank sub-grid*, fixed;
- a circular inner zone, which was identified as *Rotor sub-grid*, rotating with rotor angular velocity ω.

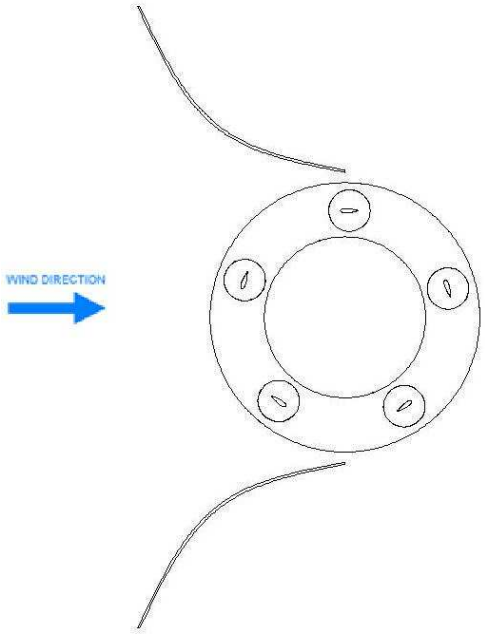

Fig. 2 Schema of shroud and rotor

Fig. 3 shows the main dimensions of the *Water Tank sub-grid* area. In order to allow a full development of the wake, Ferreira et al. [8] placed inlet and outlet boundary conditions respectively 10 diameters upwind and 14 diameters downwind with respect to rotor test section for a wind tunnel CFD simulation. In the present case, because of the huge domain width necessary to avoid solid blockage, inlet and outlet were placed respectively 37 rotor diameters upwind and 60 rotor diameters downwind with respect to the rotor test section.

Inlet was set as a *velocity inlet*, with a constant velocity profile of 2 m/s, while outlet was set as a *pressure outlet*. Two *symmetry* boundary conditions were used for the two side walls. The circumference around the circular opening, centered on the turbine rotational axis, was set as an *interface*, thus ensuring the continuity of the flow field.

The *Rotor sub-grid* is the fluid area simulating the revolution of the water turbine and is therefore characterized by a moving mesh, rotating at the same angular velocity of the turbine. Its location coincides exactly with the circular opening inside the *Water Tank sub-grid* area and is centered on the turbine rotational axis. Fig. 4 shows the main dimensions and the boundary conditions of the *Rotor sub-grid* area.

All blade profiles inside the *Rotor sub-grid* area were enclosed in a control circle of 400 mm diameter. Unlike the interface, it had no physical significance: its aim was to allow a precise dimensional control of the grid elements in the area

close to rotor blades, by adopting a first size function operating from the blade profile to the control circle itself and a second size function operating from the control circle to the whole *Rotor sub-grid* area, ending with grid elements of the same size of the corresponding *Water Tank sub grid* elements. An *interior* boundary condition was used for control circle borders, thus ensuring the continuity of the cells on both sides of the mesh.

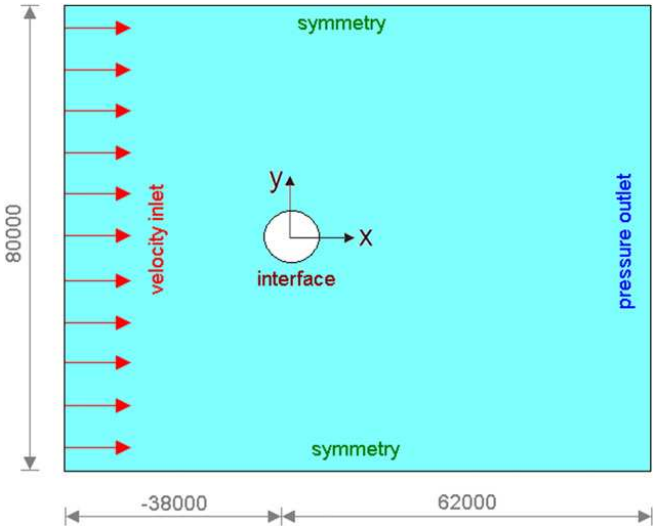

Fig. 3 Main dimensions [mm] of the *Water Tank sub-grid* area

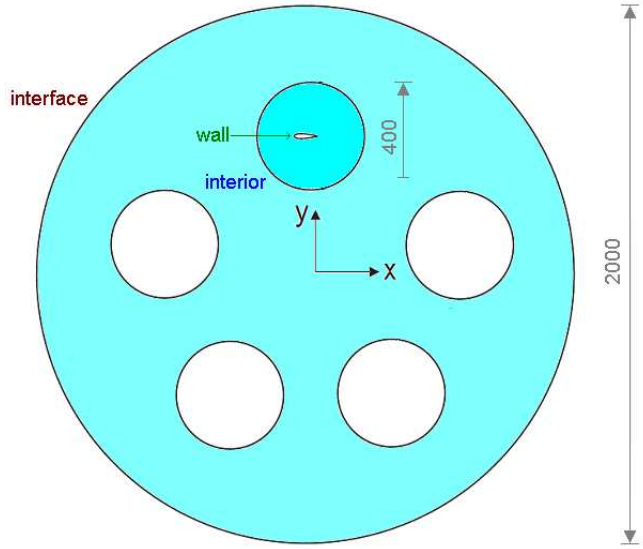

Fig. 4 Schema of the *Rotor sub-grid* area (dimensions in mm)

IV. Discretization of the Numerical Flow Field

A rotating mesh was adopted in order to represent the revolution of the VAWaterT. To discretize the flow field, an unstructured grid was chosen for the entire domain, in order to reduce the engineering time to prepare the CFD simulations. The mesh on both sides of the *interface* (*Rotor sub-grid* and *Water Tank sub-grid* areas) had approximately the same characteristic cell size in order to obtain faster convergence [9].

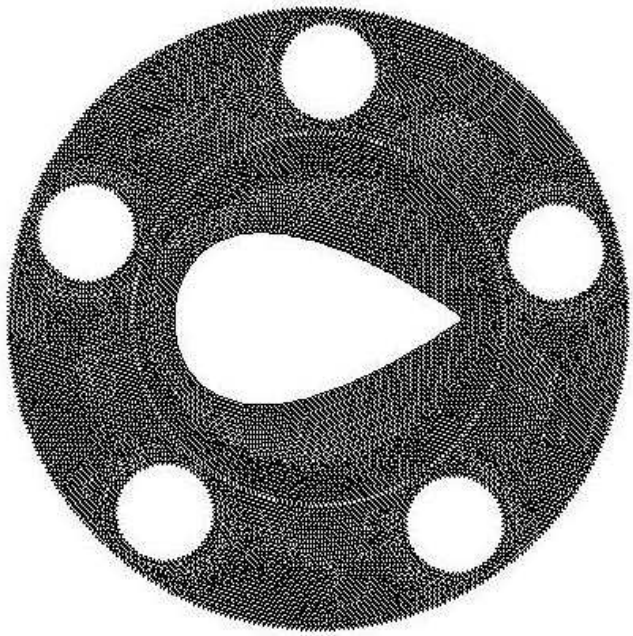

Fig. 5 *Rotor sub-grid* mesh for the shrouded configuration with NACA-shaped axis

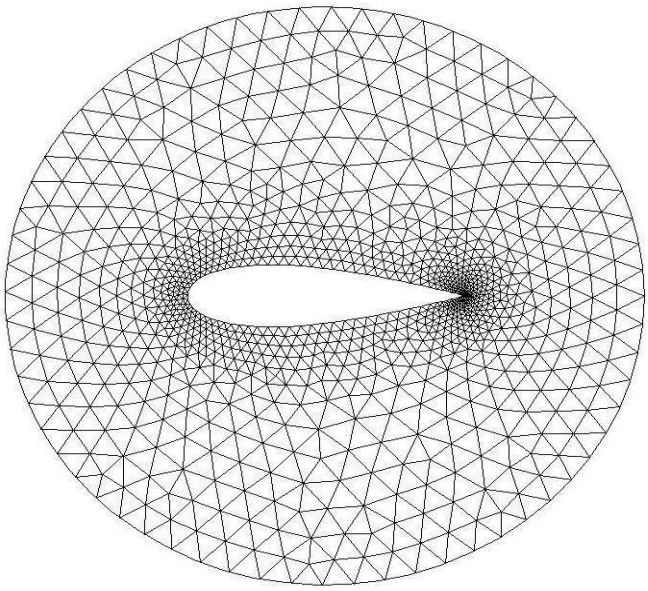

Fig. 6 Control circle grid

An isotropic unstructured mesh was chosen for the *Rotor sub-grid*, in order to guarantee the same accuracy in the prediction of rotor's performance during the revolution of the turbine (according to the studies of Commings et al. [10]) and also in order to test the prediction capability of a very simple grid. Considering their features of flexibility and adaption capability, unstructured meshes are in fact very easy to obtain, for complex geometries, too, and often represent the "first attempt" in order to get a quick response from the CFD in engineering work. The *Rotor sub-grid* mesh is represented in Fig. 5, for the shrouded configuration with NACA-shaped axis.Being the area close to the blade profiles, great attention was placed in the *control circle*. The computational grids were

constructed from lower topologies to higher ones, adopting appropriate size functions, in order to cluster grid points near the leading edge and the trailing edge of the blade profile, so as to improve the CFD code capability of determining lift, drag and the separation of the flow from the blade itself. Table II summarizes the main features of the mesh close to rotor blade, while Fig. 6 represents the control circle mesh. Fig. 7 shows the spatial domain discretization close to the shroud.

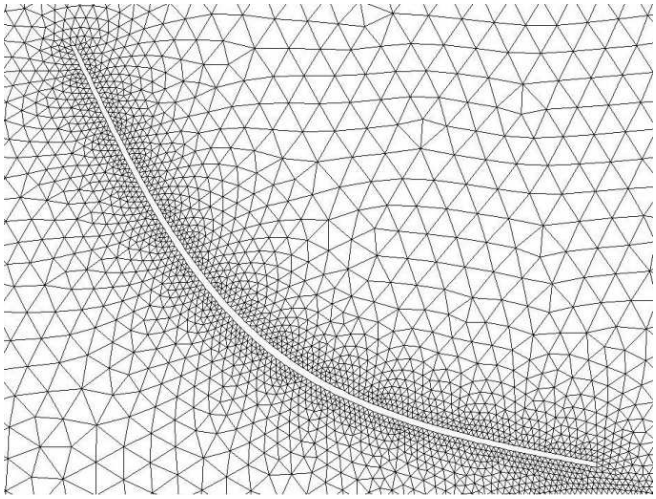

Fig. 7 Spatial domain discretization close to the shroud

TABLE II
MAIN DIMENSIONS OF THE COMPUTATIONAL DOMAIN

Denomination	Value
Starting grid size from blade leading edge [mm]	1.3
Growth factor from blade leading edge [-]	1.08
Starting grid size from blade trailing edge [mm]	0.4
Growth factor from blade trailing edge [-]	1.28
Maximum grid size on rotor blade [mm]	3.5
Growth factor from blade surface to *Rotor sub-grid* area [mm]	1.25
Maximum grid size on *Rotor sub-grid* area [mm]	10

V. Characteristics of the Numerical Simulations

A complete campaign of simulations, based on full RANS unsteady calculations, was performed for a five-bladed rotor architecture characterized by a NACA 0025 profile, in bare and shrouded configuration. The tip speed ratio, defined as:

$$\lambda = \omega \cdot R_{rotor} / V_{\infty}. \quad (1)$$

was varied from a value of $\lambda = 0.54$ (which corresponds to an angular velocity of $\omega = 2.1$ rad/s for an incoming freestream velocity of 2 m/s) to $\lambda = 2.7$ (which corresponds to an angular velocity of $\omega = 10.5$ rad/s). These conditions correspond to a range of blade Reynolds numbers from $9.25 \cdot 10^4$ to $4.63 \cdot 10^5$.

The blade Reynolds number for this work was defined as:

$$Re = (\rho \cdot R_{rotor} \cdot \omega \cdot c) / \mu \quad (2)$$

The dynamic viscosity μ was assumed to be 0.001 Pa·s, the density ρ was set to 1000 kg/m^3 and the free stream velocity V_∞ was set to 2 m/s.

VI. Numerical Solution and Convergence Criteria

As pointed out by Mc Muller et al. [11], the calculation of unsteady flows in turbo-machinery continues to present a severe challenge to CFD. During VAWaterT operation, the unsteadiness stems mainly from the relative motion of the rotating blades and has a fundamental period which depends both on the rate of rotation and on the number of blades. For the proposed calculations, the temporal discretization was achieved by imposing a physical time step equal to the lapse of time the rotor takes to make a 1° rotation.

As a global convergence criterion, each simulation was run until instantaneous torque values showed a deviation of less than 1% compared with the equivalent values of the previous period, for three consecutive periods. The period is a function of the number of blades and corresponds to a revolution of 72°, because of rotor five-bladed geometry. Residuals convergence criterion for each physical time step was set to 10^{-5} [12].

As observed by Yu et al. [13], for airfoil flows with great adverse pressure gradient and separation, the choice of a turbulence model is very important. The *k-ω SST* turbulence model can achieve good results because of its capability of capturing the proper behaviour in the near wall layers and separated flow regions. In the case of low Reynolds number, laminar-to-turbulent transition is also an important factor that should be taken into account, in order to more accurately predict the flow separation and skin friction. In the present work, the chosen turbulence model was the *k-ω SST*, that combines several desirable elements of the existing two-equation models. A 2D pressure based solver was adopted, which is well suited to solve incompressible flows [9]. The unsteady formulation was set to second-order implicit.

VII. Results and Discussion

Fig. 8 represents the evolution of the power coefficient, defined as:

$$C_p = P / (\tfrac{1}{2} \cdot \rho \cdot A_s \cdot V_\infty^3) \quad (3)$$

as a function of the tip speed ratio, for the three analyzed turbine architectures.

It can be seen that, as expected, the shrouded configurations provide a better result because of the increment of the flow speed in proximity of the rotor. The shrouded configuration without the central axis provides a peak power coefficient 60% greater than that of the bare configuration. On the contrary, the adoption of the NACA 0060 shaped central axis determines a reduction in the peak performance of the shrouded configuration of about 30%. This phenomenon could be connected to the deceleration of the flow due to the presence of the obstacle in the middle of the rotor.

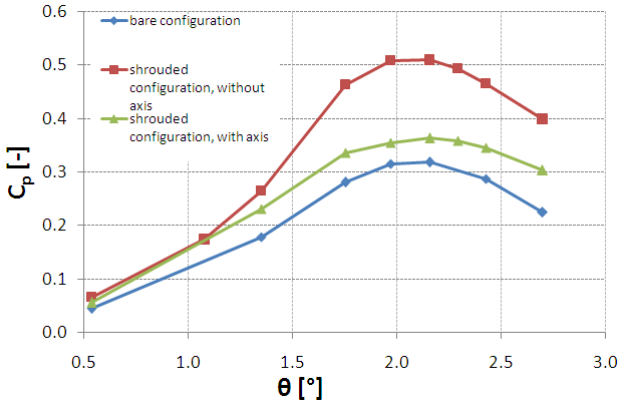

Fig. 8 Power coefficient as a function of tip speed ratio

The increment of the power coefficient obtained with the shroud is not comparable with the almost 300% increment obtained by Kirke [5]. This is due to the tested geometry of the shroud, which is not yet optimized.

The peak power coefficient is obtained for the tip speed ratio of $\lambda = 2.16$ for all the three tested cases, as already seen in [14] for the five-bladed rotor architecture.

Fig. 9 represents the torque coefficient, defined as:

$$C_t = T / (½\cdot\rho\cdot A\cdot R_{rotor}\cdot V_\infty^2) \quad (4)$$

for a single rotor blade over a full 360° revolution.

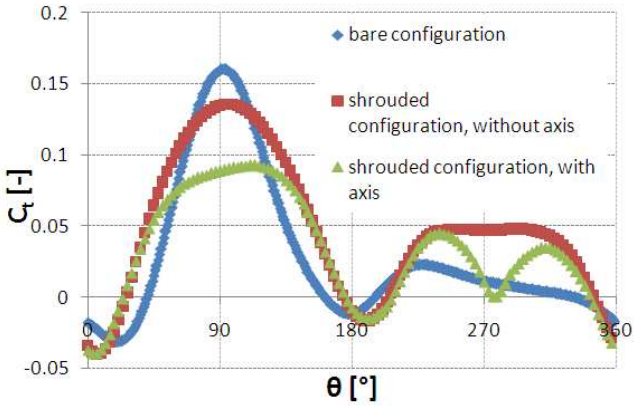

Fig. 9 Torque coefficient as a function of the angular position of blade No.1, $\lambda = 2.16$

It can be seen that the maximum torque values are generated during the upwind revolution of the turbine and for azimuthal positions where rotor blades are experiencing very high relative angles of attack, even beyond the stall limit, as already observed by Raciti Castelli et al. [12] for a wind turbine blade. It is also clear that the introduction of the shroud smoothes the torque coefficient in the upstream region, as yet observed by Roa et al. [6], and brings it to higher values in the downstream region. The introduction of the axis lowers even more the peak of the torque coefficient. It is easy to see that for the shrouded configuration with axis the torque falls to zero in the downstream region for $\theta = 279°$, when the blade travels through the turbulent zone caused by the presence of the axis.

It can also be noticed that the position of maximum torque coefficient moves to higher values of θ. Table III shows the values of peak torque coefficient with their corresponding values of θ, and the percentile differences with respect to the bare configuration.

TABLE III
VALUES OF PEAK TORQUE COEFFICIENT, CORRESPONDING ANGULAR POSITION AND PERCENTILE VARIATION WITH RESPECT TO THE BARE CONFIGURATION, $\lambda = 2.16$

Name	$C_{t,max}$ [-]	$\theta(C_{t,max})$ [°]	$\Delta C_{t,max}$ [%]
Bare configuration	0.16	92	-
Shrouded (no axis)	0.13	96	-0.19
Shrouded (with axis)	0.09	111	-0.44

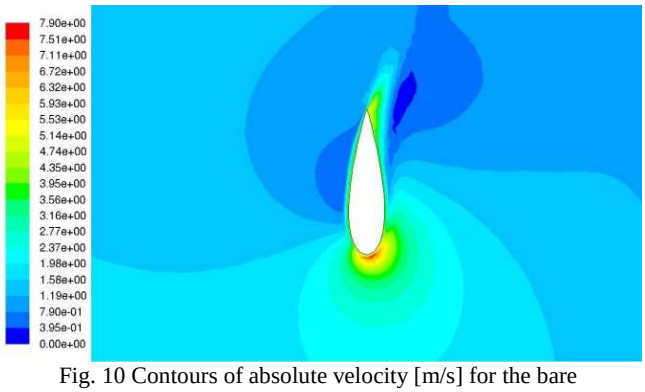

Fig. 10 Contours of absolute velocity [m/s] for the bare configuration; $\lambda = 2.16$, $\theta = 90°$

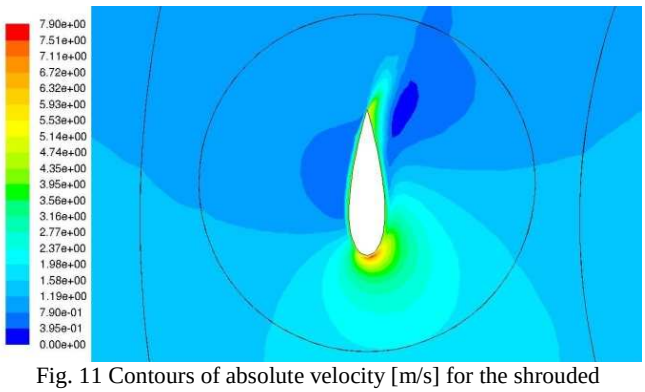

Fig. 11 Contours of absolute velocity [m/s] for the shrouded configuration without axis; $\lambda = 2.16$, $\theta = 90°$

With the exclusion of the zones near $\theta = 90$ and $\theta = 270$ (i.e. the two passages before and behind the axis), the behavior of the two shrouded configurations is almost the same and the curves representing the torque coefficient overlap. Figs. from 10 to 12 represent the contours of absolute velocity near the blade passing in the forward part of the rotor, for $\theta = 90°$.

The differences in the C_t diagrams for the three cases can be attributed not only to the increment in velocity inducted by the convergent geometry, but also to the deviation of the path-lines caused by the walls of the shroud. This last fact affects the angle of attack seen by the hydrofoils.

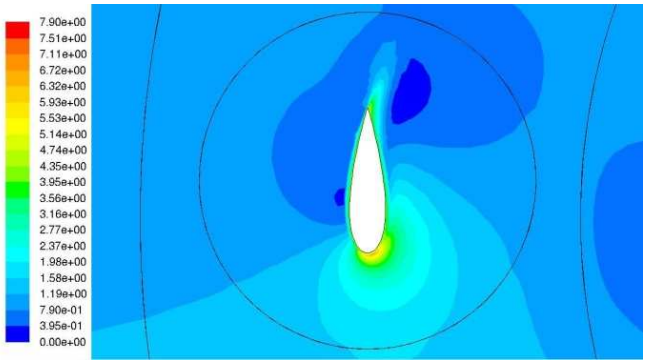

Fig. 12 Contours of absolute velocity [m/s] for the shrouded configuration with axis; $\lambda = 2.16$, $\theta = 90°$

It can be seen that the contours of velocity for the bare and shrouded (without the central axis) configurations are very similar. On the contrary, the presence of the axis determines lower values of absolute velocities. This can be due to the perturbation induced on the flow field by the presence of the axis.

Figs. from 13 to 15 present a comparison of the contours of absolute velocity for the whole rotor area.

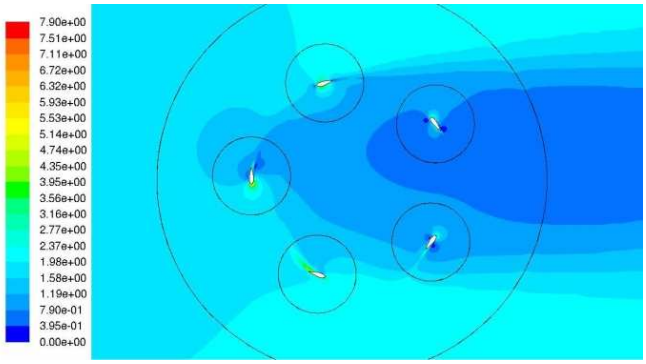

Fig. 13 Contours of absolute velocity [m/s] for the whole rotor area; bare rotor configuration, $\lambda = 2.16$, $\theta = 90°$

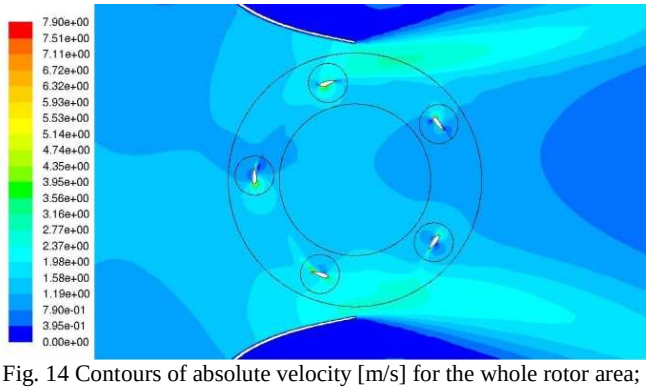

Fig. 14 Contours of absolute velocity [m/s] for the whole rotor area; shrouded rotor configuration, $\lambda = 2.16$, $\theta = 90°$

Flow acceleration due to the presence of the shroud can be clearly seen from Fig. 14, while the decelerated zone behind the axis (that produces the fall to zero of the torque coefficient for $\theta = 279°$, see Fig. 9) can be seen from Fig. 15. This phenomenon is highlighted also in Figs. from 16 to 18, where a 3D diagram of the velocity in the rotor zone is presented. Thanks to the introduction of the shroud, the velocity in the rotor zone is clearly increased (as can be seen from the green area in Fig. 17).

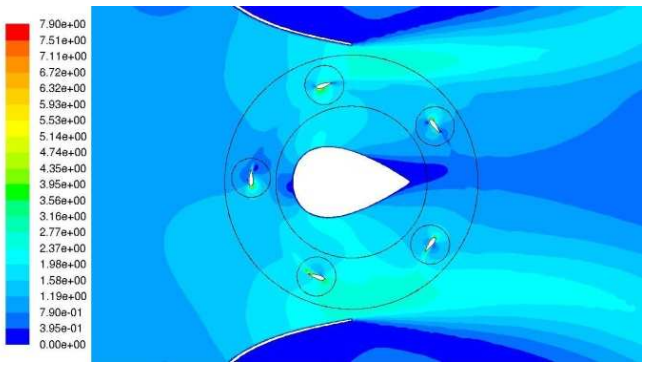

Fig. 15 Contours of absolute velocity [m/s] for the whole rotor area; shrouded rotor configuration with axis, $\lambda = 2.16$, $\theta = 90°$

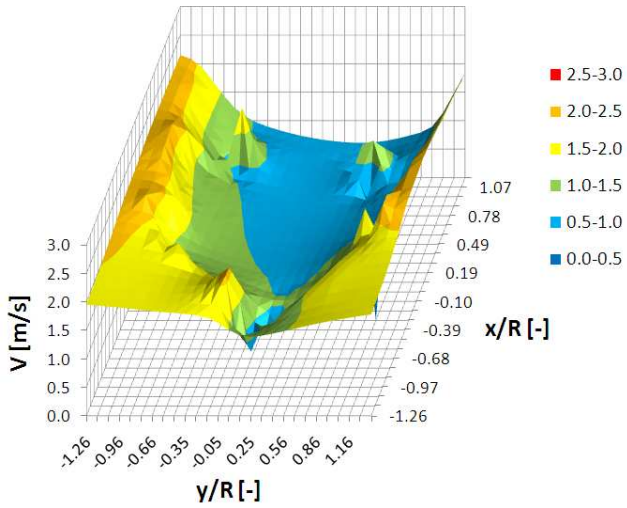

Fig. 16 Three-dimensional representation of the absolute velocity field [m/s] in proximity of the rotor; bare rotor configuration, $\lambda = 2.16$, $\theta = 90°$

The low velocity zone caused by the presence of the axis can be observed in Fig. 18. On the contrary, the lateral zones present high values of velocity (as can be seen from the red areas), produced by the blockage induced by the NACA 0060 shaped axis.

Fig. 19 presents the trend of the radial component of the fluid-dynamic resultant force on a single blade over an entire revolution. This component of the hydrodynamic force doesn't produce any effect on the torque of the rotor, but its amplitude can cause bending loads on rotor blades. It can be seen that the introduction of the shroud does not determine any significant changes in the amplitude of the radial force in the upstream region, while some increments are registered in the downstream region. Again, a drop of F_n in the passage behind the axis can be noticed for the shrouded configuration with axis. In the remaining positions, the forces for the two shrouded architectures overlap.

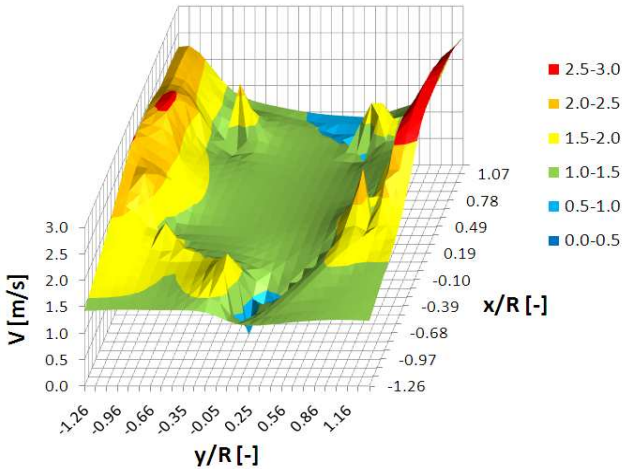

Fig. 17 Three-dimensional representation of the absolute velocity field [m/s] in proximity of the rotor; shrouded rotor configuration, $\lambda = 2.16$, $\theta = 90°$

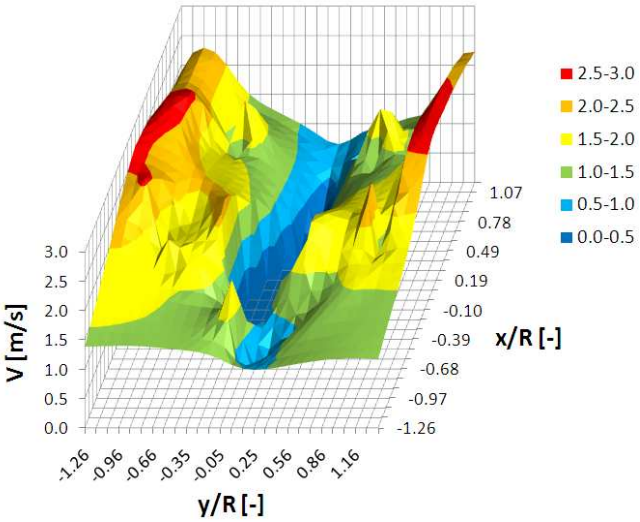

Fig. 18 Three-dimensional representation of the absolute velocity field [m/s] in proximity of the rotor; shrouded rotor configuration with axis, $\lambda = 2.16$, $\theta = 90°$

VIII. Conclusions and Future Works

Two-dimensional numerical simulations of a vertical axis water turbine in bare and shrouded configurations were performed, in order to determine the increment of performance due to the presence of the shroud. A NACA-shaped hydrofoil, representing the central axis of the rotor, was added in order to determine the effect on the overall performance of the rotor. The result of the introduction of the shroud was an increment in the power coefficient of 60% with respect to the bare configuration. The introduction of the axis lowered the performance of 30% with respect to the simple shrouded configuration.

The toque coefficient was smoothed by the introduction of the shroud in the upwind phase, but its amplitude has been increased in the downstream region. The configuration with the NACA-shaped central axis presented a marked drop of the performance in the passage behind the axis itself. The contours of absolute velocity close to rotor blades do not present significant differences between the bare and the shrouded configuration for $\theta = 90°$. On the contrary, the introduction of the axis caused a change in the contours of velocity, perturbing the flow in front of the rotor.

As expected, the velocities close to the rotor resulted much higher for the shrouded configurations. The introduction of the axis produced a slightly increment of velocity on the lateral sides of the shroud, but the overall performance resulted unsatisfying. The radial component of the fluid-dynamic force did not suffer of notable changes with the introduction of the shroud in the upstream region, and resulted increased in the downstream region.

Future work can be focus on the optimization of the geometry of the shroud, in order to enhance the performance of the system shroud-rotor. Also some combined fluid-dynamic and structural work can be done in order to determine the optimal dimension of the axis, obtaining the optimal compromise between performance of the rotor and rigidity of the structure.

Acknowledgement

The present work was developed in cooperation with Vortex Energy S.r.l. (Italy), as a part of a research project finalized to the manufacturing of a Darrieus VAWaterT.

Nomenclature

A_s [m^2]	rotor swept area
c [m]	chord length
C_t [-]	water turbine torque coefficient
$C_{t,max}$ [-]	maximum water turbine torque coefficient
C_p [-]	water turbine power coefficient
D_{rotor} [m]	Rotor diameter
F_n [N]	fluid-dynamic radial force
H_{rotor} [m]	rotor height
P [W]	water turbine power output
Re [-]	Reynolds number
R_{rotor} [m]	rotor radius
T [Nm]	water turbine torque output
V_∞ [m/s]	free water velocity
θ [°]	azimuthal position of blade No. 1 center of pressure
$\theta(C_{t,max})$ [°]	angular coordinate of maximum torque coefficient
$\Delta C_{t,max}$ [%]	torque coefficient percentage deviation
λ [-]	tip speed ratio
μ [Pa·s]	dynamic viscosity
ρ [kg/m^3]	water density
σ [-]	rotor solidity
ω [rad/s]	rotor angular velocity

References

[1] D. L. F. Gaden and E. L. Bibeau, "A numerical investigation into the effect of diffusers on the performance of hydro kinetic turbines using a validated momentum source turbine", *Journal of Renewable Energy* 35, pp. 1152-1158, 2010.

[2] M. J. Khan, G. Bhuyan, M. T. Iqbal and J. E. Quaicoe, "Hydrokinetic energy conversion systems and assessment of horizontal and vertical axis turbines for river and tidal applications: A technology status review", *Journal of Applied Energy* 86, pp. 1823-1835, 2009.

[3] S. Bernard, A. Georgescu, S. C. Georgescu, R. Susan-Resigaand and I. Anton, "Flow investigation in Achard turbine", *Proceeding of the Romanin Academi*, Series A, Volume 9, November, 2008.
[4] M. J. Khan, M. T. Iqbal and J. E. Quaicoe, "A technology review and simulation based performance analysis of river current turbine", *IEEE CCECE/CCGEI*, Ottawa, May 2006.
[5] B. Kirke, "Developments in ducted water current turbines", *Tidal paper*, 25 April 2006.
[6] A. M. Roa, V. Aumelas, T. Maitre and C. Pellone, "Numerical and experimental analysis of a Darriues-type cross flow water turbine in bare and shrouded configurations", *IOP Conf. Series: Earth and Environmental Science* 12, 2010.
[7] Maitre, T., Mentxaka Roa, A., Pellon,e C., Achard, J. L., "Numerical 2D hydrodynamic optimization of channeling devices for cross-flow water turbines", *U.P.B. Sci: Bull*. Series D, Vol. 72, Iss.1, 2010.
[8] S. Ferreira, H. Bijl, G. van Bussel and G. van Kuik, "Simulating dynamic stall in a 2D VAWT: modeling strategy, verification and validation with particle image velocimetry data", *The Science of making torque from wind. Journal of Physics*: Conference Series 75, 2007.
[9] Fluent Inc., *Fluent User's Manual*, 2006.
[10] R. M. Cummings, J. R. Forsythe, S. A. Morton and K. D. Squires, "Computational challenges in high angle of attack flow prediction", *Prog Aerospace Sci*, 2003.
[11] M. Mc Mullen, A. Jameson and J. J. Alonso, "Acceleration of convergence to a periodic steady state in turbomachinery flows", *39th AIAA aerospace sciences meeting & exhibit*. Reno, NV: AIAA; January 8-11 2001.
[12] M. Raciti Castelli, A. Englaro and E. Benini, "The Darrieus wind turbine: Proposal for new performance prediction model based on CFD", *Energy*, Volume 36, Issue 8, August 2011.
[13] G. H. Yu, X. C. Zhu and Z. H. Du, "Numerical simulation of a wind turbine airfoil: dynamic stall and comparison with experiments", *Power and Energy Journal*, Vol. 224, 2010.
[14] M. Raciti Castelli, S. De Betta and E. Benini, "Proposal for a Means for reducing the Torque Variation on a Vertical-Axis Water Turbine by Increasning the Blade Number", submitted *ICAMAME 2012: International Conference on Aerospace, Mechanical, Automotive and Materials Engineering*, Venice (Italy), April 11-13, 2012.